Theoretical modeling of the effect of plasticity on reverse transformation in superelastic shape memory alloys

Wenyi Yan*[1], Chun Hui Wang[2], Xin Ping Zhang[1] and Yiu-Wing Mai[1]

[1] Centre for Advanced Materials Technology,

School of Aerospace, Mechanical and Mechatronic Engineering,

The University of Sydney, NSW 2006, Australia

[2] Aeronautical and Maritime Research Laboratory,

Defence Science and Technology Organisation,

506 Lorimer Street, Fishermans Bend, VIC 3207, Australia

Keywords: Phase transformations; Plasticity; Shape memory alloys; Theory and modeling; Constitutive equations

* To whom all correspondence should be addressed

Abstract

Stimulated by recent experimental results on superelastic NiTi shape memory alloy, a theoretical study is carried out to quantify the effect of plasticity on stress-induced martensite transformation, using a constitutive model that combines phase transformation and plasticity. A constraint equation is introduced to quantify the phenomenon of the stabilization of plasticity on stress-induced martensite. The stabilized martensite volume fraction is determined by the equivalent plastic strain. The transformation constitutive model is adopted from a generalized plastic model with Drucker-Prager type phase transformation functions, which are pressure sensitive, while the plasticity is described by the von Mises isotropic hardening model. The martensite volume fraction is chosen as the internal variable to represent the transformation state and it is determined by the consistency transformation condition. An approach to calibrate model parameters from uniaxial tensile tests is explored, as well as the issue of elastic mismatch between austenite and martensite is discussed. Based on the proposed constitutive model, the influence of hydrostatic stress on transformation is examined. As an example of application, this new constitutive model is employed to numerically study the transformation field and the plastic deformation field near a crack tip.

1. Introduction

It is well known that shape memory alloys exhibit not only shape memory effect but also superelastic deformation behavior. At a certain high temperature, shape memory alloy under external loading can display extraordinarily large deformation, up to strains of several percents. This large amount of deformation can “elastically” recover completely after unloading. This abnormal superelastic phenomenon is due to the intrinsic stress-induced austenite-to-martensite forward transformation and martensite-to-austensite reverse transformation during a loading-unloading process. The transformation deformation mechanism is schematically illustrated in Fig. 1. The initial austenite phase can be transformed into martensite phase under external force. Due to different crystal structures between the austenite and the martensite, deformation

occurs during the phase transformation process, which leads to significant macroscopic deformation. Once the transformed material is unloaded, the unstable martensite phase will transform backward to the stable austenite recovering the transformation strain.

The superelastic deformation behaviour in shape memory alloys has been exploited to develop smart and functional structures in many fields [1-3]. Of particular importance is its exciting application in the field of biomedical engineering. For example, superelastic NiTi vascular stents have been developed to reinforce blood vessels. Comparing to traditional stainless steel stents, these superelastic stents have enhanced recoverable strain so that they can be easily deployed to constricted arteries and the risk of stent failure would be greatly reduced [4, 5]. In addition, further potential applications of shape memory alloys are being investigated, such as shape memory alloys-based functional composites. Recent reports, e.g., [6], suggest that shape memory alloy NiTi has super resistance against wear due to its superelasic deformation and could be applied in tribological engineering.

Although shape memory alloy NiTi has found many important applications, especially in biomedical engineering, little information on the failure of this material existed in the literature. McKelvey and Ritchie [7, 8] carried out a series of experimental study on the growth of fatigue cracks in NiTi alloy. With regarding to the constitutive behaviors of this material, they have experimentally found that plastic deformation after forward transformation could stabilize martensite and hinder the reverse transformation. Eventually, reverse transformation can be suppressed completely with a certain amount of plastic deformation. They have also reported that austenite-to-martensite forward transformation did not occur at the crack tip of a superelastic NiTi. The inhibition of the transformation was believed to be due to the high hydrostatic tensile stress near the tip of at a fatigue crack. Because the austenite-to-martensite transformation in NiTi involves a negative volume change, the high hydrostatic tensile stress might prevent such transformation from happening.

Stimulated by the experimental investigation of McKelvey and Ritchie [7, 8] on superealstic NiTi, the authors present a constitutive model, which can describe not only superelastic transformation but also plastic

deformation, especially the effect of plastic deformation on the stabilization of martensite so that it can be applied to theoretically study the failure of superelastic shape memory alloys. Many constitutive models for transformation in shape memory alloys have been published [2, 9]. Transformation thermomechanical theory, crystallographic theory of martensitic transformation and/or micromechanics approach have been applied to develop some of these models [10-13]. For the purpose of our present research, a phenomenological model developed by Auricchio et al. [14] and Lubliner and Auricchio [15] was modified to describe forward and reverse transformation in superelastic shape memory alloys. Without detailing the evolution process of the material microstructure, this model can phenomenologically quantify the macroscopic deformation due to transformation. And, this model was successfully applied to numerically simulate the deformation of NiTi stents recently by Rebelo et al. [16]. In contrast to many other models, this phenomenological model has also considered the volume change during transformation process. Thus, it can be used to study the influence of hydrostatic stress on transformation. The von Mises isotropic hardening theory is adapted directly to describe the plastic deformation happening in the martensite phase after the forward transformation. The stabilized martensite volume fraction is proposed as a function of the equivalent plastic strain. Therefore, the constraint of the plastic deformation on the reverse transformation can be quantified.

The structure of this paper is as follows. The combined constitutive model is detailed in Section 2, where the evolution functions of the martensite volume fraction are derived based on the consistency conditions. Thereafter, the transformation strain rate is determined. For the sake of completeness, the equation to determine the plastic strain rate is also given in Section 2. A simple linear relationship is proposed between the stabilized martensite volume fraction and the equivalent plastic strain. Methods of calibrating the material parameters from uniaxial tensile tests are outlined in Section 3. Based on the present model, the effect of hydrostatic stress on transformation has been discussed. This constitutive model has been implemented as a material subroutine in the finite element package ABAQUS [17] to assist the analysis of the transformation and plastic deformation of a superelastic structure under complex loading condition.

Finally, as an example of application, the transformation field and the plastic field near the crack tip of a superelasitc NiTi shape memory alloy is examined in Section 4.

2. Constitutive model

Under external loading condition, the total strain rate of a superelastic material generally composes of three parts:

$$\dot{\boldsymbol{\varepsilon}} = \dot{\boldsymbol{\varepsilon}}^{el} + \dot{\boldsymbol{\varepsilon}}^{tr} + \dot{\boldsymbol{\varepsilon}}^{pl} \tag{1}$$

where $\dot{\boldsymbol{\varepsilon}}^{el}$ is elastic strain rate due to elastic deformation, $\dot{\boldsymbol{\varepsilon}}^{tr}$ transformation strain rate due to transformation and $\dot{\boldsymbol{\varepsilon}}^{pl}$ plastic strain rate due to dislocation movement. Plastic deformation due to dislocation movement is unrecoverable, whereas elastic and transformation strains are recoverable. During unloading process, reverse transformation from martensite to austenite can occur in the superelastic regime, which partly or fully recovers the deformation due to the forward transformation from austenite to martensite. Here, only mechanical loading condition for transformation is considered and the forward and reverse transformation is treated as an isothermal process. These constraints could be removed by introducing relevant temperature-dependent parameters. Because plastic yield strength is normally higher than the transformation stress in shape memory alloys, unlike transformation-induced plasticity in steels, transformation and plastic deformation will not occur simultaneously for shape memory alloy. The following details a combined constitutive model that describes both the transformation strain and plastic strain.

In the present work, both austenite and martensite are considered to be elastic isotropic. The elastic strain rate $\dot{\boldsymbol{\varepsilon}}^{el}$ is related to the stress rate via the isotropic Hooke's law:

$$\dot{\boldsymbol{\varepsilon}}^{el} = \mathbf{M} : \dot{\boldsymbol{\sigma}}, \tag{2}$$

where $\mathbf{M}$ is the elastic isotropic flexibility tensor of the fourth-order and $\dot{\boldsymbol{\sigma}}$ is the stress rate tensor. It is further assumed that austenite and martensite have identical elastic properties (Young's modulus and Poisson's ratio). For copper-based shape memory alloys, the difference of the Young's modulus between the

martensite and the austenite is negligibly small. By contrast, for binary NiTi shape memory alloys the Young's modulus of the martensite is about one-third to one half of the Young's modulus of the austenite [18]. Normally, the transformation strain rate is much larger than the elastic strain rate during a transformation process, either forward transformation or reverse transformation. The elastic mismatch between austenite and martensite can only affect the macroscopic deformation very limitedly even for NiTi shape memory alloys. While this difference can be readily incorporated in the theoretical model, the resulting model may require more elaborate experiments to identify the material constants; this will be discussed in detail in the next section.

2.1 Transformation model

To avoid the complexity of tracking the detailed evolution of the material microstructure during phase transformations, a phenomenological approach will be adopted to describe the forward and reverse transformation in superelastic shape memory alloys. Such an approach is most appropriate for polycrystalline shape memory alloys with very fine grains, such as NiTi used in stent device. Here the model developed by Auricchio et al [14] and Lubliner and Auricchio [15] is modified in a consistent manner to account for multiaxial stresses. The martensite volume fraction rate will be determined from a self-consistency condition, rather than assuming an empirical relation in [14,15].

Choosing the martensite volume fraction f as an internal state variable, which varies between zero and unity. The potential functions for forward and reverse transformations are a Drucker-Prager type, *i.e.*

$$F_{for}(\boldsymbol{\sigma}, f) = \sigma_{eq} + 3\alpha\sigma_m - Y_{for}(f), \text{ for forward transformation} \tag{3a}$$

$$F_{rev}(\boldsymbol{\sigma}, f) = \sigma_{eq} + 3\alpha\sigma_m - Y_{rev}(f), \text{ for reverse transformation} \tag{3b}$$

where $\sigma_{eq} = \sqrt{\frac{3}{2}\mathbf{s}:\mathbf{s}}$ is the von Mises equivalent stress, $\mathbf{s}$ is the deviatoric stress tensor, and σ_m is the hydrostatic stress, *i.e.*,

$$\sigma_m = \frac{1}{3} tr(\boldsymbol{\sigma}) \quad \text{and} \quad \mathbf{s} = \boldsymbol{\sigma} - \sigma_m \mathbf{I} \tag{4}$$

where $\mathbf{I}$ is the second-order unit tensor. The function $Y_{for}(f)$ and $Y_{rev}(f)$ denote the transformation hardening functions to be determined later. Generally, these hardening functions also depend on temperature. Here, investigation is focused on a given temperature, at which material demonstrates superelastic behavior. The influence of the hydrostatic stress on transformation is manifested by the term $\alpha\sigma_m$ in Eq. (3). The parameter α is a material constant, which is relative to the transformation volume strain as discussed later. In the case of $\alpha = 0$, the transformation function degenerate to the von Mises type.

During phase transformation the potentials $F_{for}(\boldsymbol{\sigma}, f)$ and $F_{rev}(\boldsymbol{\sigma}, f)$ remain zero. It will prove advantageous to define an equivalent transformation stress σ_{eq}^{tr} as

$$\sigma_{eq}^{tr} = \sigma_{eq} + 3\alpha\sigma_m . \tag{5}$$

Then the conditions for transformation can be simply expressed as,

$$\sigma_{eq}^{tr} = Y_{for}(f), \text{ for forward transformation} \tag{6a}$$

$$\sigma_{eq}^{tr} = Y_{rev}(f), \text{ for reverse transformation} \tag{6b}$$

which are similar to the plastic yield criterion in conventional plasticity theory.

During forward transformation process, the martensite volume fraction increases, i.e., $\dot{f} > 0$. Similarly, decreasing of the martensite volume fraction, $\dot{f} < 0$, indicates a reverse transformation process. It is assumed that the transformation strain rate is proportional to the martensite volume fraction rate $\dot{f}$. According to the normality hypothesis, the transformation strain rate $\dot{\boldsymbol{\varepsilon}}^{tr}$ during forward transformation process can be determined by:

$$\dot{\boldsymbol{\varepsilon}}^{tr} = \beta\dot{f}\frac{\partial F_{for}}{\partial \boldsymbol{\sigma}} = \beta\dot{f}\left(\frac{3}{2}\frac{\mathbf{s}}{\sigma_{eq}} + \alpha\mathbf{I}\right), \quad \dot{f} > 0 . \tag{7a}$$

During reverse transformation process, it is:

$$\dot{\boldsymbol{\varepsilon}}^{tr} = \beta \dot{f} \frac{\partial F_{rev}}{\partial \boldsymbol{\sigma}} = \beta \dot{f} \left(\frac{3}{2} \frac{\mathbf{s}}{\sigma_{eq}} + \alpha \mathbf{I} \right), \quad \dot{f} < 0 . \tag{7b}$$

The parameter β is a material constant, which can be calibrated from uniaxial tensile test as discussed in the next section.

The martensite (transformed) volume fraction rate $\dot{f}$ can be determined by the consistency conditions as in classical plasticity theories [19]. The consistency condition for transformation is

$$\dot{F} = \frac{\partial F}{\partial \boldsymbol{\sigma}} : \dot{\boldsymbol{\sigma}} + \frac{\partial F}{\partial f} \dot{f} = 0 \tag{8}$$

from which the martensite volume fraction rate $\dot{f}$ can be obtained as

$$\dot{f} = \frac{1}{H_{for}} \left(\frac{3}{2} \frac{\mathbf{s} : \dot{\mathbf{s}}}{\sigma_{eq}} + 3\alpha \dot{\sigma}_m \right), \quad \dot{f} > 0 \quad \text{for forward transformation} \tag{9a}$$

$$\dot{f} = \frac{1}{H_{rev}} \left(\frac{3}{2} \frac{\mathbf{s} : \dot{\mathbf{s}}}{\sigma_{eq}} + 3\alpha \dot{\sigma}_m \right), \quad \dot{f} < 0 \quad \text{for reverse transformation} \tag{9b}$$

where $H_{for} = \frac{dY_{for}}{df}$ and $H_{rev} = \frac{dY_{rev}}{df}$ represent the forward transformation hardness and the reverse transformation hardness, respectively.

2.2 Plastic strain rate

Generally, plastic yield stress is higher than the critical stress for forward martensitic transformation in shape memory alloys. After finishing forward transformation, plastic deformation can occur in the stress-induced martensite if the external force increased continuously over the plastic yield strength of the martensite phase. The isotropic hardening theory based on von Mises yielding condition is the mostly used model to describe the plastic deformation of normal metals. This model is adopted directly here to describe the plastic behavior of stress-induced martensite. The plastic yield condition is

$$F_{pl}(\boldsymbol{\sigma}, \bar{\varepsilon}^{pl}) = \sigma_{eq} - Y_{pl}(\bar{\varepsilon}^{pl}) = 0, \tag{10}$$

where Y_{pl} is the plastic hardening function of the material, which depends on the equivalent plastic strain $\bar{\varepsilon}^{pl}$. The equivalent plastic strain $\bar{\varepsilon}^{pl}$ is defined by the plastic strain tensor $\boldsymbol{\varepsilon}^{pl}$ through

$$\bar{\varepsilon}^{pl} = \int_{\text{history}} \sqrt{\frac{2}{3} d\boldsymbol{\varepsilon}^{pl} : d\boldsymbol{\varepsilon}^{pl}}\,. \tag{11}$$

The plastic strain rate can be determined by

$$\dot{\boldsymbol{\varepsilon}}^{pl} = \frac{9}{4}\frac{\mathbf{s}}{\sigma_{eq}^2 H_{pl}} \mathbf{s} : \dot{\mathbf{s}}, \tag{12}$$

where $H_{pl} = \dfrac{dY_{pl}}{d\bar{\varepsilon}^{pl}}$ is the plastic hardness, which is treated as a material parameter.

It is worthy to mention that a non-linear kinematic hardening law demonstrating the Bausinger effect will be a better choice for the purpose of describing the plastic deformation behavior under cyclic loading condition such as the cases in wear study. Efficient numerical algorithms for implementing this class of constitutive model have been developed [20] and a numerical wear model based on the failure of plastic deformation accumulation is available [21]. Quantitatively evaluating the wear behavour of superelastic NiTi shape memory alloy is being carried out.

2.3 Influence of plastic deformation on reverse transformation

Recently, McKelvey and Ritchie [8] observed monoclinic martensitic structure in an unloaded NiTi superelastic bar after having experienced stress-induced forward transformation and plastic deformation. Furthermore, they have found that the heavier plastic deformation occurred, the less strain due to forward transformation could recover. In other words, plastic deformation could stabilize the stress-induced martensite so that no or only part reverse transformation back to austenite will occur after the removal of load. This influence of plastic deformation on the reverse transformation of NiTi shape memory alloy can be represented by the stabilized irrecoverable martensite volume fraction f_{sta}. Quantitatively, f_{sta} is assumed to be dependent on the level of prior plastic strain, i.e.,

$$f_{sta} = F(\bar{\varepsilon}^{pl}). \tag{13}$$

The function $F(\bar{\varepsilon}^{pl})$ can be calibrated from measured strain curves from uniaxial tensile tests, such as the curve of recovery strain versus applied strain shown in Fig. 12 of McKelvey and Ritchie (2001). A linear relation given below would be the simplest between f_{sta} and $\bar{\varepsilon}^{pl}$,

$$f_{sta} = \begin{cases} \dfrac{\bar{\varepsilon}^{pl}}{\bar{\varepsilon}_c^{pl}}, & \bar{\varepsilon}^{pl} \le \bar{\varepsilon}_c^{pl} \\ 1, & \bar{\varepsilon}^{pl} > \bar{\varepsilon}_c^{pl} \end{cases} \tag{14}$$

where $\bar{\varepsilon}_c^{pl}$ is the minimum plastic strain after which no reverse transformation will occur at all.

This influence of plastic deformation on the ability of martensite to undergo reverse transformation places an important condition on the evolution of the martensite volume fraction *f*. In other words, the following condition should also be satisfied during reverse transformation ($\dot{f} < 0$),

$$f > f_{sta}. \tag{15}$$

This means that f_{sta} essentially serves as a lower bound for reverse transformation.

3. Calibration of Material Parameters

Uniaxial test is a basic experimental approach to study material constitutive behavior and to calibrate material parameters. The constitutive model presented in the previous section will first specialized to uniaxial loading to assist the identification of the relevant material parameters. The elastic properties of the austenite and the martensite are assumed to be identical within acceptable prediction accuracy. Possible difficulties in calibrating parameters due to elastic mismatch will discussed later. Based on the present model, the influence of hydrostatic stress on transformation is also examined.

3.1 Transformation parameters α and β

Since the plastic yield stress of NiTi shape memory alloys is higher than the critical forward transformation stress, it is possible to determine the transformation parameters α and β from superelastic deformation tests before plastic deformation occurs. The influence of plastic deformation on the reverse transformation of martensite can be determined separately.

According to Eq. (7), the transformation strain rate consists of two parts, deviatoric component $\frac{3}{2}\frac{\mathbf{s}}{\sigma_{eq}}\beta\dot{f}$ and volumetric component $\beta\dot{f}\alpha\mathbf{I}$. When the martensite volume fraction *f* reaches unity, the maximum forward transformation volume strain from austenite to martensite can be obtained by integrating the volumetric term in equation (7), which is

$$\varepsilon_v^{tr} = 3\alpha\beta . \tag{16}$$

This maximum transformation volume strain can be calculated by applying crystallographic theory for martensitic transformation based on the structure change of the two phases or be measured directly from experiments. For examples, the maximum transformation volume strain for CuAlNi shape memory alloy is –0.37% according to the calculation of Fang et al [22]; and Holtz et al [23] measured the value of ε_v^{tr} for NiTi shape memory alloy, which is about -0.39%.

Under the uniaxial tensile loading condition, the maximum transformation strain in the tensile direction is, after integrating equation (7),

$$\varepsilon_{11}^{tr} = \beta(1+\alpha) . \tag{17}$$

By combining Eqs (16) and (17), the parameters α and β can be determined once the values of ε_v^{tr} and ε_{11}^{tr} are known. Take as an example of the NiTi superelastic shape memory alloy studied by McKelvey and Ritchie [8], ε_{11}^{tr} was measured to be about 4.0% from a uniaxial tensile test. Together with $\varepsilon_v^{tr} = -0.39\%$ from [23], one can derive the following solutions

$$\alpha = -3.15\% \quad \beta = 4.13\% . \tag{18}$$

Corresponding to equivalent plastic strain in traditional plasticity (see Eq. (11)), an equivalent transformation strain $\bar{\varepsilon}^{tr}$ can be defined as follows:

$$\bar{\varepsilon}^{tr} = \frac{1+\alpha}{\sqrt{1+2\alpha^2}} \int_{histroy} \sqrt{\frac{2}{3} d\dot{\boldsymbol{\varepsilon}}^{tr} : d\dot{\boldsymbol{\varepsilon}}^{tr}} = \beta(1+\alpha) \int_{histroy} |df| . \tag{19}$$

Obviously, it is equal to the transformation strain component ε_{11}^{tr} in the case of uniaxial tensile loading condition.

3.2 Transformation hardening functions

If the non-zero stress component is denoted by σ_{11} in a uniaxial tensile test, according to Eqs (6), during forward transformation process we have

$$Y_{for}(f) = (1+\alpha)\sigma_{11} . \tag{20}$$

In the mean time, based on Eq. (7a), in the tensile direction can be expressed as

$$\dot{\varepsilon}_{11}^{tr} = \beta(1+\alpha)\dot{f} . \tag{21}$$

Because the elastic Young's modulus of the martensite is assumed to be the same of the austenite, the elastic strain rate still linearly depends on the stress rate during transformation process. Therefore, the transformation strain rate $\dot{\varepsilon}_{11}^{tr}$ can be extracted from the total strain rate $\dot{\varepsilon}_{11}$ by

$$\dot{\varepsilon}_{11}^{tr} = \dot{\varepsilon}_{11} - \dot{\varepsilon}_{11}^{el} = \dot{\varepsilon}_{11} - \frac{\dot{\sigma}_{11}}{E} . \tag{22}$$

In calibrating the transformation hardness, for a given stress increment $\Delta\sigma_{11}$, as illustrated by Fig. 2, after measuring the corresponding total strain increment $\Delta\varepsilon_{11}$ from the stress-strain curve, the transformation strain increment $\Delta\varepsilon_{11}^{tr}$ can be deducted from Eq. (22). After that, the increment of the martensite volume fraction Δf can be obtained from Eq. (21). Because the value of the transformation hardening function $Y_{for}(f)$ is determined by Eq. (20), the functional relation between $Y_{for}(f)$ and f can be determined point by

point starting from the initial transformation point $f = 0$ and $\sigma_{11} = \sigma_0$ at the stress-total strain curve. The reverse transformation hardening function $Y_{rev}(f)$ can be calibrated in the similar way based on the stress-strain curve in the reverse transformation process.

If the measured stress-strain curve in the forward transformation regime can be correlated by a linear relationship,

$$\sigma_{11} = \sigma_0 + C_{for}\ (\varepsilon_{11} - \frac{\sigma_0}{E}), \tag{23}$$

where $C_{for} = \dot{\sigma}_{11} / \dot{\varepsilon}_{11}$ is a constant, which represents the tangential modulus as shown in Fig. 2, a simple analytical expression for the transformation hardening function $Y_{for}(f)$ can be obtained. According to (9a), for the forward transformation under uniaxial tension, we have

$$\dot{f} = \frac{(1+\alpha)}{H_{for}} \dot{\sigma}_{11}. \tag{24}$$

Therefore, the total strain rate in the tensile direction can be expressed as

$$\dot{\varepsilon}_{11} = \dot{\varepsilon}_{11}^{el} + \dot{\varepsilon}_{11}^{tr} = \frac{\dot{\sigma}_{11}}{E} + \beta(1+\alpha)\dot{f} = \frac{\dot{\sigma}_{11}}{E} + \frac{\beta(1+\alpha)^2 \dot{\sigma}_{11}}{H_{for}}. \tag{25}$$

From Eq. (25), we have

$$H_{for}(f) = \frac{C_{for}\beta\,(1+\alpha)^2}{1 - C_{for}/E}. \tag{26}$$

In this special case, $H_{for}(f)$ is a constant value. According to the definition of $H_{for}(f)$, we have

$$Y_{for}(f) = \int H_{for}(f) df = (1+\alpha)\sigma_0 + \frac{C_{for}\beta(1+\alpha)^2}{1 - C_{for}/E} f. \tag{27}$$

A similar linear expression for the reverse transformation hardening function $Y_{rev}(f)$ can be obtained if the part of the stress-strain curve can be approximated by a straight line.

For the material properties listed in Table 1 which were determined from the experimental results of McKelvey and Ritchie [8] based on the above described approach, the calculated stress-strain curve under uniaxial loading condition is shown in Fig. 3. In this case, the applied stress is lower than the plastic yield strength. No plastic deformation occurs and reverse transformation can occur completely after unloading.

Under uniaxial compression with the amplitude σ_{11}, the transformation conditions are

$$Y_{for}(f) = \sigma_{eq}^{tr} = (1-\alpha)\sigma_{11} \ , \text{ for forward transformation} \tag{28a}$$

$$Y_{res}(f) = \sigma_{eq}^{tr} = (1-\alpha)\sigma_{11} \ , \text{ for reverse transformation.} \tag{28b}$$

It is clear that for the same martensite volume fraction, the stress amplitude to trigger transformation under compression is different from that under tension. The stress-strain curve in Fig. 3 shows asymmetry about the origin point. Due to volume contraction during forward transformation for shape memory alloys, the parameter α turns out to be negative. Therefore, the amplitude of the transformation stress under compression is lower than that under tension in uniaxial loading condition for the same martensite volume fraction, as shown in Figure 3.

3.3 Plastic constraint

McKelvey and Ritchie [8] measured the variation of the recovery strain with the applied total strain in their uniaxial tensile tests. The results suggested that the recovery strain decreased sharply after plastic deformation. The minimum plastic strain to totally stabilize martensite ($\bar{\varepsilon}_c^{pl}$) is about 0.84%. Martensite will not transform back to austenite once material experiences plastic strain over this value. The linear function of Eq. (14) can be applied to approximate the relation between the stabilized martensite volume fraction f_{sta} and the experienced plastic deformation $\bar{\varepsilon}^{pl}$. Figure 4 shows the influence of plasticity on reverse transformation deformation at different loading levels under uniaxial tensile condition. These curves are predicted using the combined constitutive model. In the first case, the applied maximum stress in less than the plastic yield strength, and no plastic deformation occurs. Martensite can transform completely back to

austenite as the force unloads to zero, i.e. $f_{sta} = 0.0$. In the second case as marked by the dashed curve, the plastic strain of 0.41% causes a volume fraction 49.0% of the martensite phase is stabilized. The total residual strain is 2.4% at zero stress, much greater than the applied plastic strain. When the applied plastic strain exceeds the critical value of 0.84%, reverse transformation is completely constrained, as indicated by the dotted curve in Fig.4.

3.4 Effect of elastic mismatch

In the present model, the austenite phase and the martensite phase are assumed to have identical elastic properties. In principle, however, there is no difficulty in allowing the elastic mismatch of the two phases during transformation process. A simple way is to apply the linear mixture rule to evaluate the Young's modulus *E* of the bi-phase material,

$$E = (1-f)E_a + fE_m, \tag{29}$$

where E_a and E_m are respectively the Young's moduli of the austenite and the martensite, and *f* is the volume fraction of the martensite. The Poisson's ratios can be still considered as the same or be treated using a similar linear mixture rule. The elastic mismatch will not affect transformation model and the plastic constraint equation in Section 2. However, in doing so, the calibration of material parameters will be complicated.

Suppose that the elastic Young's moduli of the austenite and the martensite are different, the averaged Young's modulus based on Eq. (29) is a function of the martensite volume fraction *f*, which changes with the stress state. During uniaxial tensile loading process, the total strain rate can now be expressed as follows:

$$\dot{\varepsilon}_{11} = \dot{\varepsilon}_{11}^{el} + \dot{\varepsilon}_{11}^{tr} = \frac{\dot{\sigma}_{11}}{(1-f)E_a + fE_m} + \beta(1+\alpha)\dot{f}\,. \tag{30}$$

The elastic strain rate will no longer linearly depend on the stress rate during transformation process. Therefore, it is difficult to extract the transformation strain from the measurable total strain unless the

volume fraction of the martensite could be determined during the transformation process. Practically, it is a challenging task to measure the volume fraction of the martensite.

Figure 5 schematically illustrates a typical superelastic curve for NiTi, which manifests the difference of elastic Young's moduli. Similar experimental curves can be found in the literature [8, 24]. Here, A_s and A_f represent respectively the starting point and the finishing point of the forward transformation; and R_s the reverse transformation starting point, R_f the reverse finishing transformation point. Due to superelastic deformation, a closed hysteretic loop exists, which can be described by

$$\varepsilon_a^{el} + \varepsilon_{for}^{el} + \varepsilon_{for}^{tr} = \varepsilon_m^{el} + \varepsilon_{rev}^{el} + \varepsilon_{rev}^{tr}, \tag{31}$$

where ε_a^{el} is the elastic strain created from R_f to A_s, ε_{for}^{el} the elastic strain during forward transformation from A_s to A_f, ε_{for}^{tr} the forward transformation strain, ε_m^{el} the elastic strain amplitude from A_f to R_s, ε_{rev}^{el} the elastic strain amplitude during reverse transformation from R_s to R_f and ε_{rev}^{tr} the reverse transformation strain amplitude. Generally, ε_{for}^{el} is close to ε_{rev}^{el} because the transformation hardening effect is typically small. Therefore, the following approximation relation can be obtained,

$$\varepsilon_a^{el} + \varepsilon_{for}^{tr} = \varepsilon_m^{el} + \varepsilon_{rev}^{tr}. \tag{32}$$

For NiTi shape memory alloys, the Young's modulus of the martensite is one-third to one half of that of the austenite for NiTi. Therefore, ε_m^{el} can be much larger than ε_a^{el}, which is can be shown in Fig. 5. In other words, we have such conclusion,

$$\varepsilon_{for}^{tr} > \varepsilon_{rev}^{tr}. \tag{33}$$

It means that the elastic strain has "consumed" part of the forward transformation strain during unloading process before reverse transformation starts at point R_s, and the total forward transformation strain is "not equal" to the total reverse transformation strain even so the reverse transformation is obviously finished completely. This deduction seems to be unacceptable.

In reality, the reverse transformation might have already started before reaching the corner point R_s. In this case, it is practically difficult to determine precisely the onset of reverse transformation. It might also be possible that the macroscopic transformation strain rate is not proportional to the transformation volume fraction rate due to twinning phenomenon between different martensite variants. Further experiments should be designed to explain the "non-equilibrium" between the forward transformation strain and reverse transformation strain, and so as to establishing appreciated mathematical models to quantify this phenomenon. It is worthy to reiterate that the model in Section 2 can successfully describe superelastic deformation within acceptable accuracy although it neglects the elastic mismatch.

3.5 Effect of hydrostatic stress

The equivalent transformation stress $\sigma_{eq}^{tr} = \sigma_{eq} + 3\alpha\sigma_m$ in (5) is the transformation driving force, where $3\alpha\sigma_m$ represents the contribution from the hydrostatic stress. Similar relation has been used by Spitzig and Richmond [25] to study the effect of pressure on the flow stress of iron-based bcc materials, where pressure influences the dislocation motion. Here, the effect of the hydrostatic stress creates due to the transformation-induced volume change, which is represented by the parameter α. The value of the parameter α is negative for shape memory alloys. It is expected pure hydrostatic pressure will contribute to the transformation driving force. In other words, if a uniaxial test were carried out with a hydrostatic compression, the critical tensile stress to trigger transformation would decrease with increasing hydrostatic pressure. To our knowledge, so far no such experiment has been reported. But, the effect of hydrostatic pressure was examined in an alternative way by Kakeshita et al [26]. They experimentally studied the influence of the hydrostatic pressure on the transformation temperature. For thermoelastic martensitic transformation occurring in shape memory alloys, not only mechanical loading but also thermal loading by reducing temperature can drive transformation. Because the hydrostatic pressure can increase the forward transformation driving force, it is expected that under higher hydrostatic pressure less transformation thermal loading is needed, i.e., martensitic transformation can occur at higher temperature. Indeed, they have found

the transformation temperature increased linearly with increasing pressure for some NiTi shape memory alloys.

On the other hand, hydrostatic tensile stress should resist transformation. In fracture mechanics, triaxial hydrostatic constraint is normally quantified in terms of the ratio of the hydrostatic stress to the von Mises equivalent stress, σ_m / σ_{eq}. Focusing on forward transformation, the onset of phase transformation can be rewritten as

$$1 + 3\alpha \frac{\sigma_m}{\sigma_{eq}} = \frac{Y_{for}(0.0)}{\sigma_{eq}}, \tag{34}$$

which means that the higher the triaxility ratio σ_m / σ_{eq}, the more difficult it is to trigger forward transformation. The influence of triaxiality also strongly depends on the value of the material parameter α. Because the transformation volume strain is much smaller than stress-induced transformation shear strain in shape memory alloys, according to Eqs. (16) and (17),, the amplitude of α is much smaller than 1.0, which is –3.15% in the above considered case. Thus, the influence of the triaxiality on transformation should be rather limited.

McKelvey and Ritchie [8] found that forward transformation did not occur ahead of the crack tip in their experiment. They hypothesized that the high hydrostatic tensile stress at the crack tip suppressed the transformation due to negative transformation volume strain. Since the triaxiality σ_m / σ_{eq} ahead of a three-dimensional crack is about 3.0 [27], and that the term $Y_{for}(0.0)/\sigma_{eq}$ is approximately zero at the crack tip due to the singular behaviour of σ_{eq} at the crack tip, the value of α should be around –11.0% in order to completely suppress phase transformation at the crack tip. This corresponds about –1.5% transformation volume contracting. This amplitude is much larger than the measured value of -0.39% in NiTi shape memory alloy. In a separate test, based on the measured macroscopic stress-strain curves, McKelvey and Ritchie concluded that forward transformation could not occur in a notched tensile bar even with

$\sigma_m / \sigma_{eq} = 1.1$. Clearly further experimental studies are needed to investigate the sensitivity of the hydrostatic tensile stress on forward phase transformation.

4. Phase Transformation and Plastic Deformation at the Tip of a Tensile Crack

The constitutive model outlined in Section 2 has been implemented as a user material subroutine for the finite element code ABAQUS [17] to analyse the phase transformation and plastic deformation of a superelastic structure under complex loading condition. Here as an example of application, the transformation and plastic deformation field near the tip of a tensile crack in a NiTi superelastic shape memory alloy is analyzed. In this case, a semi-infinite plane-strain crack subjected to remote K_I field is considered. Due to symmetry, only a half of the whole model is simulated. Figure 6(a) shows the entire mesh and the boundary condition. For a given value of K_I, the corresponding displacement field is imposed on the boundary far away from the crack tip. Here the value of K_I is chosen as 60 $\text{MPa}\sqrt{\text{m}}$. A very fine mesh is employed near the crack tip, which is illustrated in Fig. 6(b). The material constants calibrated in Section 3 are used in the calculation.

Figure 7(a) shows the distribution of the martensite volume fraction, *f*, near the crack tip under the given value of K_I. It shows that there exists a full transformed zone very close to the crack tip with *f* reaching to the maximum value 1.0. Outside that region, the martensite volume fraction reduces gradually with the distance away from the crack tip. As indicated in this figure, the normalized height of the transformation zone, $\frac{y_{tr}}{[K_I / Y_{pl}(0)]^2}$, at the contour line $f = 0.25$ is 0.90. The total normalized height of the transformation zone is 2.1. Figure 7(b) shows the distribution of the triaxial hydrostatic constraint, σ_m / σ_{eq}, near the crack tip. It indicates the highest value of σ_m / σ_{eq} is about 4.15, comparing with a value of 3.0 for a crack in a non-transformation material, which appears just in front of the crack tip. Comparing Figures 7(a) and 7(b), which are in the same scale, one can see that there exist regions near the crack tip with σ_m / σ_{eq} being less

than 0.76 while transformation having completed with $f = 1.0$. Even if the critical hydrostatic constraint to suppress transformation is as low as 1.1 as determined by the notched tensile bar test from [8], it seems that transformation could still occur in the region with lower σ_m / σ_{eq} near the crack tip, which might affect the failure behavior of the superelastic material as the influence of transformation on the toughness in ZrO2 ceramics [28, 29].

Figure 8(a) shows the plastic deformation field near the crack tip. As Figures 7 and 8 are in the same scale, it clearly indicates that the plastic zone is much smaller than the transformation zone near the crack tip. The normalized plastic zone height, $\frac{y_{pl}}{[K_I / Y_{pl}(0)]^2}$, is 0.12. Comparatively, the estimated value from linear elastic fracture mechanics is about 0.13 [30]. In this case, the phase transformation has little effect on the size of the plastic zone because the plastic yield strength is much larger than the transformation stress. The distribution of the stabilized martensite volume fraction due to plastic transformation is shown in Fig. 8(b). Stabilized martensite near the crack tip may have significant influence on the fatigue crack growth in this kind of materials. Applying fracture mechanics, the influence of transformation, plastic deformation and plastic stabilized martensite on fracture and fatigue behavior is being carried out.

5. Conclusions

The influence of plastic deformation on reverse transformation in superelastic shape memory alloys has been quantified by a constitutive model that accounts for both phase transformation and plasticity. A macroscopic phenomenonological model based on generalized plastic theory is adopted to describe the superelastic deformation behaviour. The forward and reverse transformation process is described by the change of the martensite volume fraction, which is determined by the consistency transformation condition. This transformation model involves the change of material volume due to transformation. It can account for the influence of hydrostatic stress on transformation conditions. The effect of the plasticity on the transformation is manifested by a constraint equation, which determines the stabilized martensite volume fraction to escape

reverse transformation. The present constitutive model has been applied to investigate the crack-tip deformation behaviour of a tensile crack in a superelastic shape memory alloy.

Acknowledgements

This work was financially supported by the ARC Large Research Grant (A10009166). Y-W Mai wishes to thank the Australian Research Council for the award of a Federation Fellowship tenable at the University of Sydney.

References

[1] H. Funakubo, Shape Memory Alloys. Gordon and Bleach, New York, 1987, p. 270.

[2] V. Birman, Appl. Mech. Rev. 50 (1997) 629.

[3] J. Van Humbeeck, Mater. Sci. Eng. A273-275 (1999) 134.

[4] T. W. Duerig, A. R. Pelton, D. Stoeckel, Mater. Sci. Eng. A273-275 (1999) 149.

[5] T. W. Duerig, A. R. Pelton, D. Stoeckel, Bio-Medical Mater.Eng. 6 (1996) 255.

[6] D. Y. Li, Smart Mater. Struct. 9 (2000) 717.

[7] A. L. McKelvey, R. O. Ritchie, J. Biomedical Mater. Res. 47 (1999) 301.

[8] A. L. McKelvey, R. O. Ritchie, Metall. and Mater. Trans. A32 (2001) 731.

[9] F. D. Fischer, Q.-P. Sun, K. Tanaka, Appl. Mech. Rev. 49 (1996) 317.

[10] C. Liang, C. A. Rogers, J. Intelligent Mat. Syst. Struct. 1 (1990) 207.

[11] Q.-P. Sun, K.-C. Hwang, J. Mech. Phys. Solids, 41 (1993) 1.

[12] E. Patoor, A. Eberhardt, M. Berveiller. Arch. Mech. 40 (1988) 775.

[13] W. Yan, Q.-P. Sun, K.-C. Hwang, Science in China (Series A) 28 (1998) 275.

[14] F. Auricchio, R. L. Taylor, J. Lubliner, Comput. Methods Appl. Mech. Engrg 146 (1997) 281.

[15] J. Lubliner, F. Auricchio, Int. J. Solids Struct. 33 (1996) 991.

[16] N. Rebelo, N. Walker, H. Foadian, in 2001 ABAQUS User's Conference 2001.

[17] ABAQUS Version 5.8. Providence, RI: HKS Inc. 1998.

[18] D. E. Hodgson, M. H. Wu, R. J. Biermann, Shape memory alloys, in: Metals Handbook. 10th editon, v. 2. American Society for Metals. Cleverland, Ohio. 1991. pp.897-902.

[19] J. Lemaitre, J.-L. Chaboche, Mechanics of Solid Materials. Cambridge University Press. 1990, p. 556.

[20] C. H. Wang, W. Hu, J. Sawyer, Computational Mechanics 26 (2000) 140.

[21] W. Yan, E. P. Busso, N. P. O'Dowd, Proceedings of Royal Society London, Series A456 (2000) 1.

[22] D.-N. Fang, W. Lu, W. Yan, T. Inoue, K.-C. Hwang, Acta mater. 47 (1999) 269.

[23] R. L. Holtz, K. Sadananda, M. A. Imam, Int. J. of Fatigue 21 (1999) s137.

[24] P. H. Lin, H. Tobushi, K. Tanaka, T. Hattori, M. Makita, J. Intell. Mater. Syst. Struct. 5 (1994) 694.

[25] W. A. Spitiz, O. Richmond, Acta Metall. 32 (1984) 457.

[26] T. Kakeshita, K. Shimizu, S. Nakamichi, R. Tanaka, S. Endo, F. Ono, Materials Transactions, JIM 33 (1992) 1.

[27] W.Yan, G. Shan, O. Kolednik, F. D. Fischer, Key Engineering Materials 145-149 (1998) 179.

[28] R. M. McMeeking, A. G. Evans, J. Am. Ceram. Soc. 65 (1992) 242.

[29] B. Budiansky, J. W. Hutchinson, J. C. Lambropoulos, Int. J. Solids Struct. 19 (1983) 337.

[30] T. L. Anderson, Fracture Mechanics: Fundamentals and Applications. Second Edition, CRC Press, Boca Raton, USA.1995, p. 793.

Table 1. Part material data of a NiTi superelastic SMA calibrated from [8].

E	$Y_{for}(0)$	$Y_{for}(0.6)$	$Y_{for}(1)$	$Y_{res}(1)$	$Y_{res}(0.85)$	$Y_{res}(0)$	$Y_{pl}(0)$	$Y_{pl}(0.32\%)$	$Y_{pl}(0.84\%)$	$Y_{pl}(1.68\%)$	$Y_{pl}(2.70\%)$
62 GPa	394 MPa	397 MPa	402 MPa	213 MPa	203 MPa	179 MPa	1058 MPa	1100 MPa	1167 MPa	1233 MPa	1267 MPa

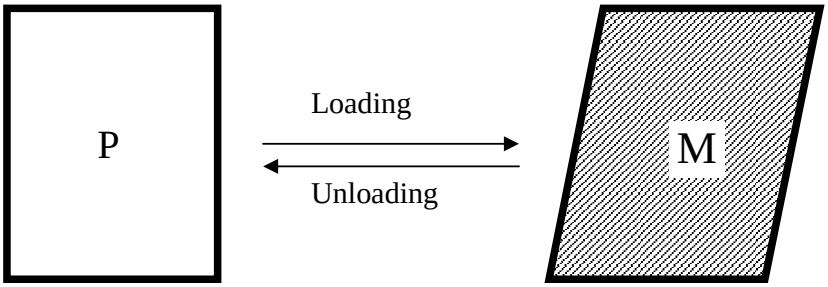

Figure 1. Illustrating superelastic deformation mechanism.

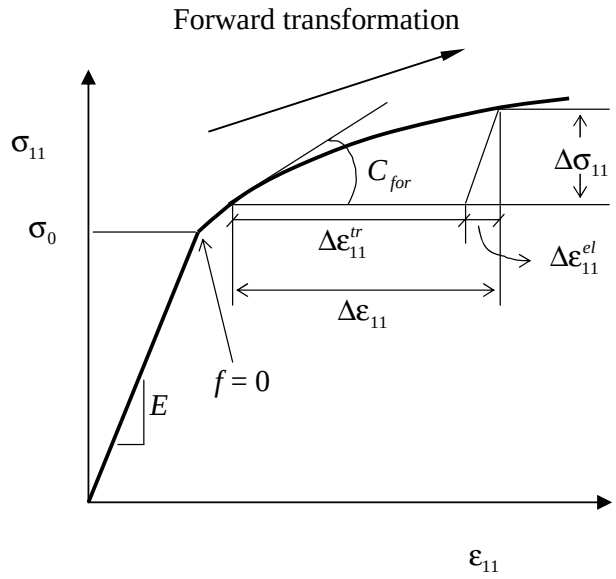

Figure 2. Illustration of the calibration process for the forward transformation hardening function from a uniaxial tensile stress-strain curve.

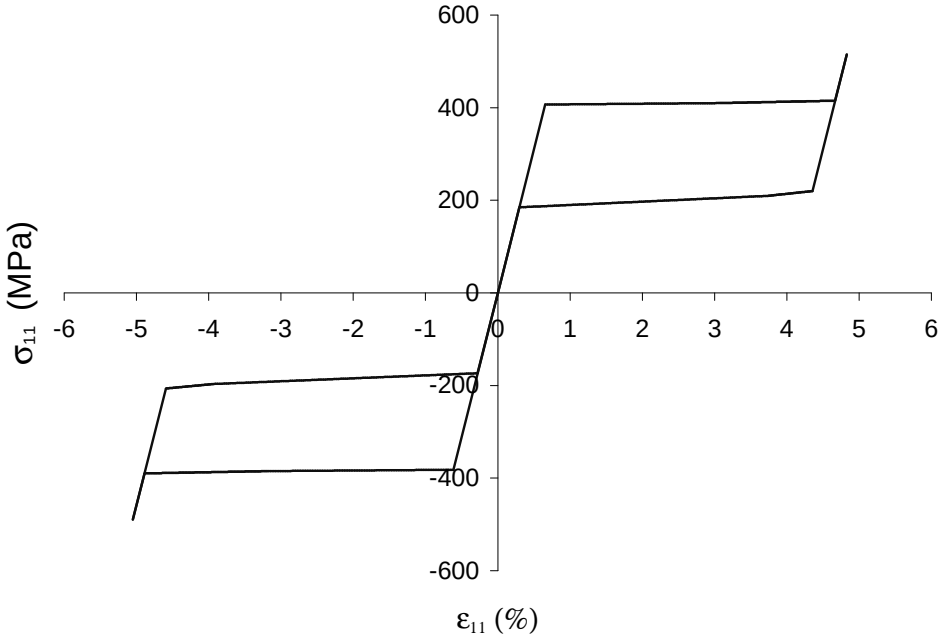

Figure 3. Predicted superelasticity under uniaxial loading condition.

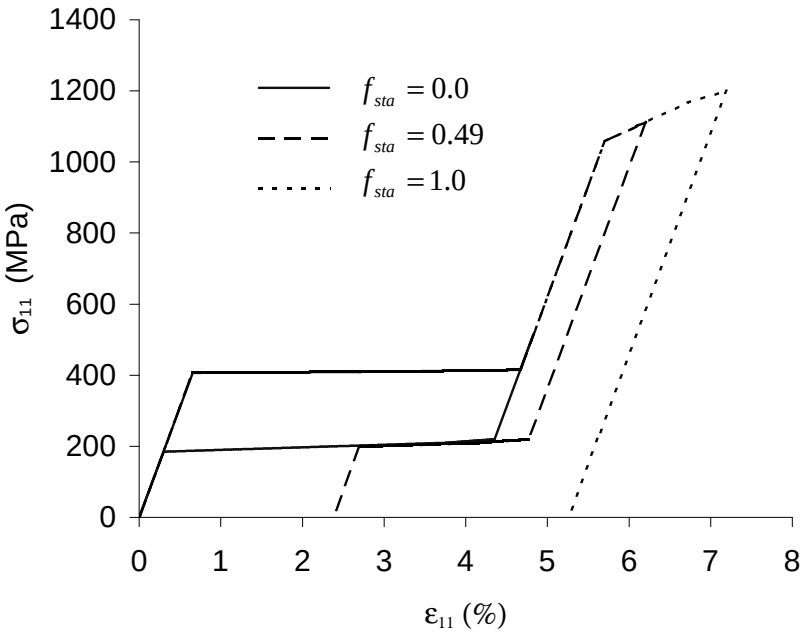

Figure 4. Stabilized martensite volume fractions due to different plastic deformation amplitude and their influences on stress-strain curves under uniaxial tension condition.

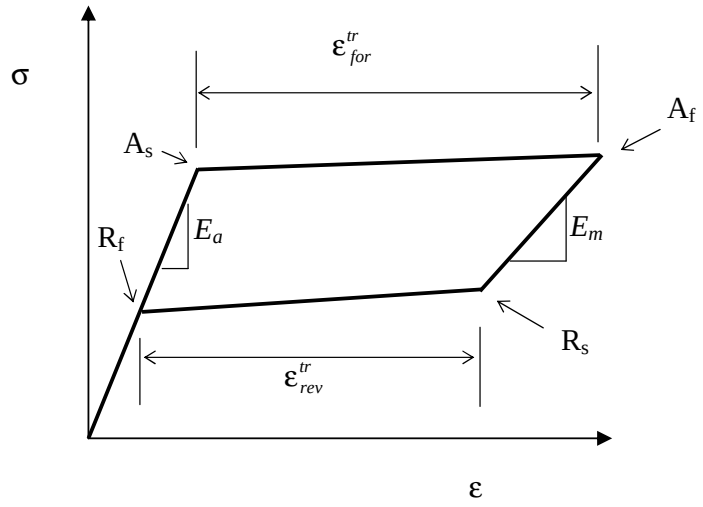

Figure 5. Schematic illustrating the “non-equilibrium” between the forward and reverse transformation strains in a typical uniaxial tensile test.

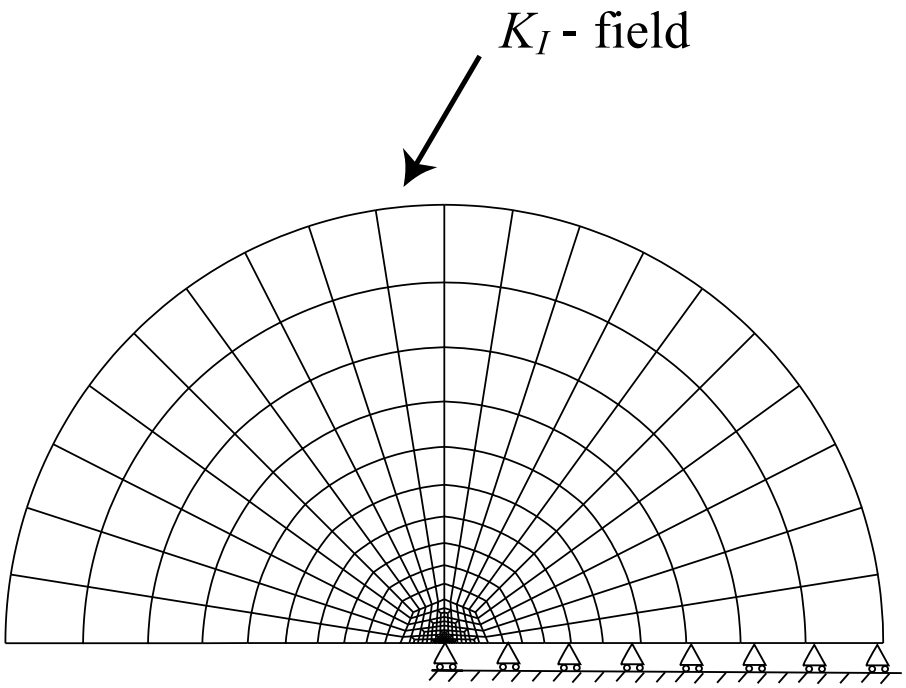

(a)

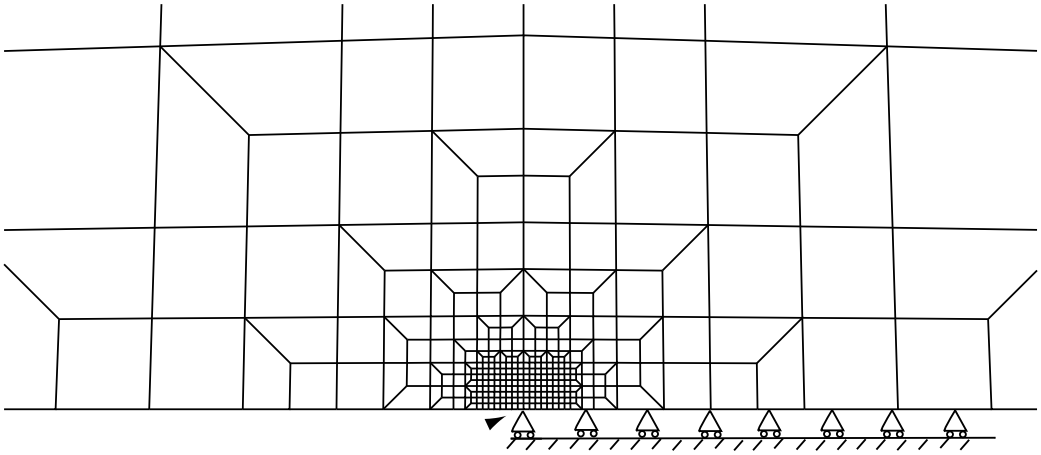

(b)

Figure 6. Finite element model for an infinite plane strain crack in a superelastic shape memory alloy subjected to remote K_I field force: (a) entire finite element mesh and boundary conditions; (b) fine mesh near the crack tip.

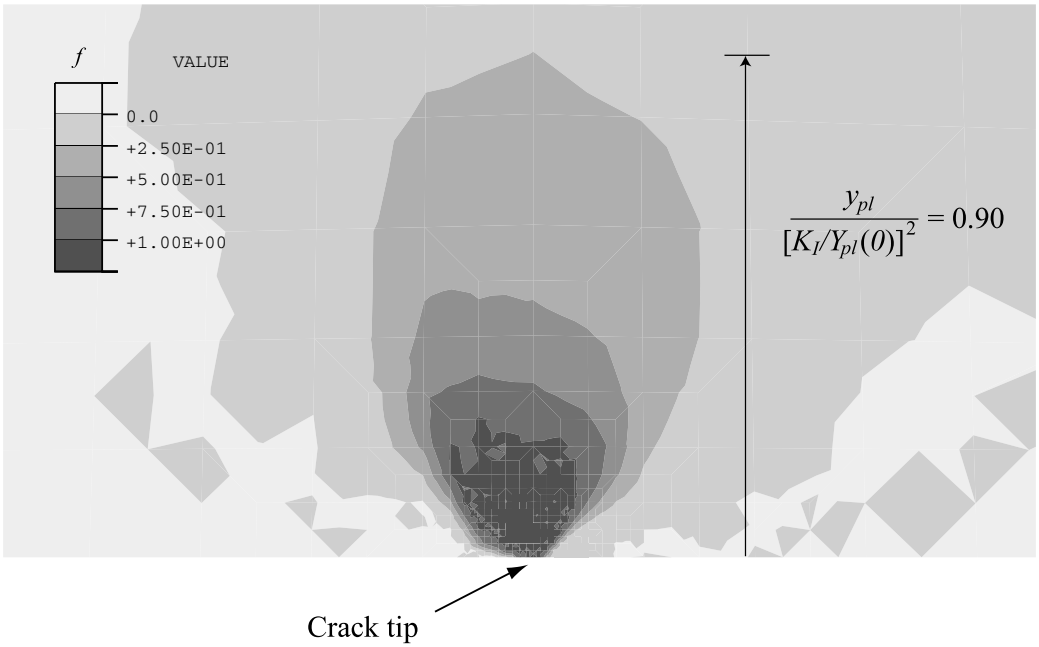

(a)

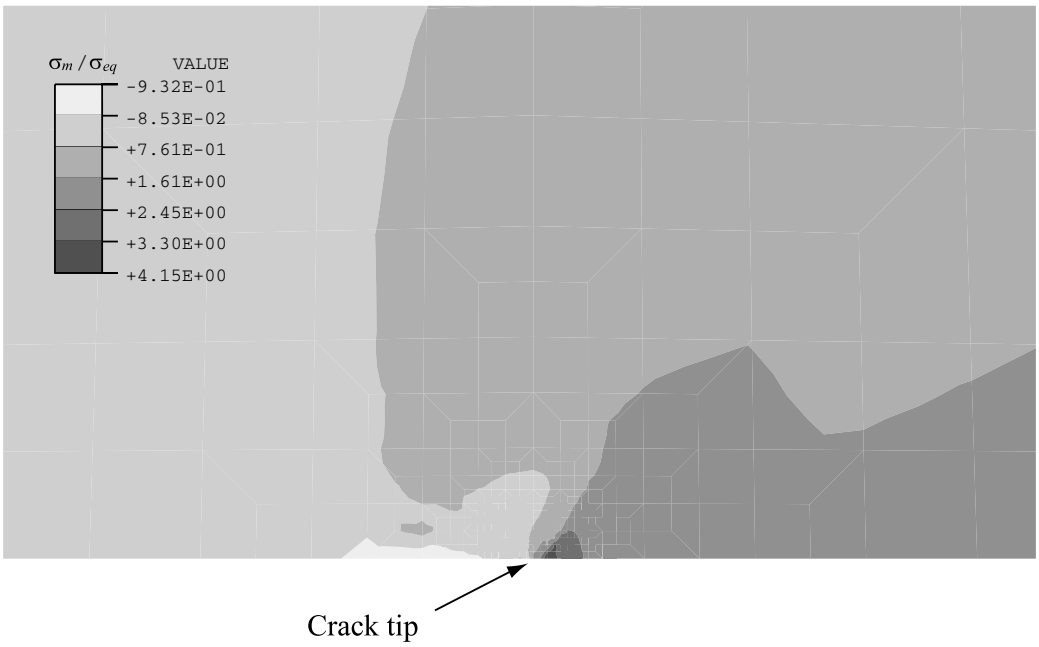

(b)

Figure 7. (a) Distribution of martensite volume fraction, f, near the crack tip; (b) Distribution of triaxial hydrostatic constraint, σ_m / σ_{eq} , near the crack tip. Figures (a) and (b) are in the same scale.

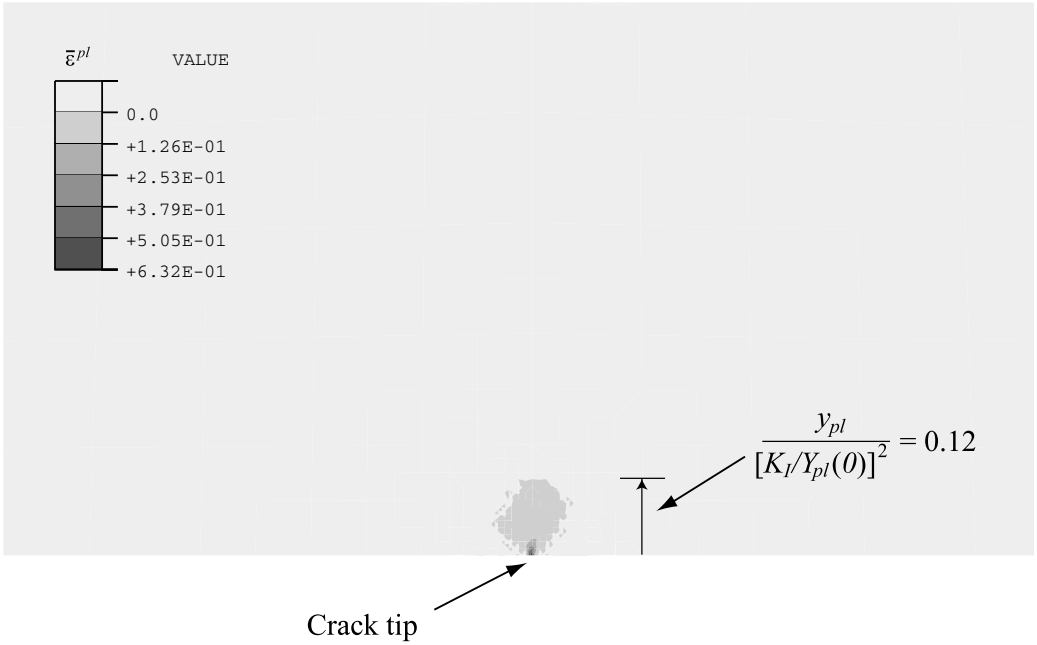

(a)

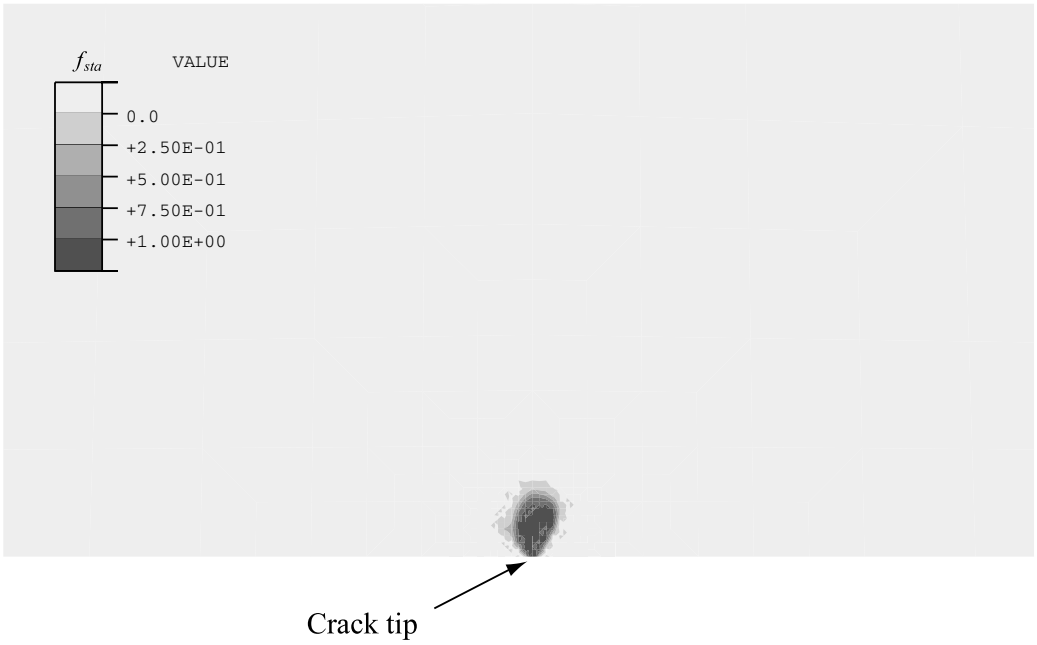

(b)

Figure 8. (a) Distribution of Equivalent plastic strain, $\bar{\varepsilon}^{pl}$, near the crack tip; (b) Distribution of stabilized martensite volume fraction, f_{sta}, near the crack tip. Figures (a) and (b) are in the same scale.